Targeting the ubiquitin-proteasome system in a pancreatic cancer subtype with hyperactive MYC

Katharina Lankes[1], Zonera Hassan[1], María Josefina Doffo[2], Christian Schneeweis[1], Svenja Lier[1], Rupert Öllinger[3,4], Roland Rad[3,4], Oliver H. Krämer[5], Ulrich Keller[2,4], Dieter Saur[4,6], Maximilian Reichert[1,4], Günter Schneider[1,4] and Matthias Wirth[2] (iD)

1 Klinik und Poliklinik für Innere Medizin II, Technical University of Munich, Munich, Germany
2 Hematology, Oncology and Tumor Immunology, Charité - Universitätsmedizin Campus Benjamin Franklin, Berlin, Germany
3 Institute of Molecular Oncology and Functional Genomics, Technical University Munich, Munich, Germany
4 German Cancer Research Center (DKFZ), German Cancer Consortium (DKTK), Heidelberg, Germany
5 Department of Toxicology, University Medical Center, Mainz, Germany
6 Institute for Translational Cancer Research and Experimental Cancer Therapy, Technical University Munich, Munich, Germany

The myelocytomatosis oncogene (MYC) is an important driver in a sub-type of pancreatic ductal adenocarcinoma (PDAC). However, MYC remains a challenging therapeutic target; therefore, identifying druggable synthetic lethal interactions in MYC-active PDAC may lead to novel pre-cise therapies. First, to identify networks with hyperactive MYC, we pro-filed transcriptomes of established human cell lines, murine primary PDAC cell lines, and accessed publicly available repositories to analyze transcrip-tomes of primary human PDAC. Networks active in MYC-hyperactive subtypes were analyzed by gene set enrichment analysis. Next, we per-formed an unbiased pharmacological screen to define MYC-associated vul-nerabilities. Hits were validated by analysis of drug response repositories and genetic gain- and loss-of-function experiments. In these experiments, we discovered that the proteasome inhibitor bortezomib triggers a MYC-associated vulnerability. In addition, by integrating publicly available data, we found the unfolded protein response as a signature connected to MYC. Furthermore, increased sensitivity of MYC-hyperactive PDACs to borte-zomib was validated in genetically modified PDAC cells. In sum, we pro-vide evidence that perturbing the ubiquitin–proteasome system (UPS) might be an option to target MYC-hyperactive PDAC cells. Our data pro-vide the rationale to further develop precise targeting of the UPS as a sub-type-specific therapeutic approach.

1. Introduction

Pancreatic ductal adenocarcinoma (PDAC) is estimated to become the second leading cause of cancer-related death. In contrast to other solid tumors, its prognosis still remains extremely poor [1]. The disease is characterized by a profound intertumoral heterogeneity [2]. Based on various technologies including mRNA sequencing, metabolite profiling, or exon sequencing, distinct molecular subtypes of PDAC associated with different prognosis, biology, and therapeutic responses have been described [2–13]. These data suggest the development of biomarker-driven therapeutic concepts as a promising approach to improve the outcome of the disease. Signatures predicting sensitivity toward the current standard of care chemotherapies are under development [12].

Whole-exome sequencing of microdissected PDAC specimen revealed that amplification of *MYC* (*c-MYC*) is the only copy number variation associated with lower survival rates [14]. These data demonstrate that myelocytomatosis oncogene (MYC) drives an aggressive subtype of the disease and consistently MYC activity was found to be enriched in the squamous/basal-like/glycolytic subtype [7,13]. MYC is involved in a variety of biological processes in cancer cells [15]. It is a prominent oncogene acting in concert with mutated *KRAS* in PDAC [16–18]. The transcription factor MYC is an intrinsically disordered protein. Although progress has been made to target MYC [19,20], it remains a challenge. A strategy to target 'undruggables' is to exploit specific cellular dependencies associated with the activity of these proteins [21]. Several unbiased genetic screens for synthetic lethal interactions have demonstrated that the MYC protein family confers targetable dependencies [22–26], pointing to a way to define precise therapies. Consistently, MYC has been connected to the increased sensitivity of bromodomain and extra terminal motif (BET) inhibitors [27,28] and inhibitors of the small-ubiquitin-like modifier (SUMO) pathway in the context of PDAC [29].

To find MYC-associated vulnerabilities, we conducted a limited drug screen and found a connection of MYC to the unfolded protein response (UPR) and an increased sensitivity toward proteasome inhibitors.

2. Materials and methods

2.1. Analysis of publicly available expression data, drug sensitivity data, and clinical data

RNA-expression data of pancreatic cancer cell lines, included in the CCLE dataset (19Q3), were downloaded from the depmap data portal (https://depmap.org/). Drug sensitivities of human PDAC cell lines from the PRISM repurposing primary screen (19Q3) [30], the GDSC2 screen (AUC) [31], and the CTD^2 (AUC) screen [32] were directly accessed and downloaded via the depmap data portal. Bortezomib sensitivity of the lines was divided into quartiles, and the most sensitive quartile was investigated for pathway enrichment using gene set enrichment using the complete CCLE-PDAC dataset. For the analysis of drug-MYC interactions, we accessed the Discriminant Regulon Expression Analysis (DoRothEA) database [33] (http://dorothea.opentargets.io/) and extracted significant (FDRq < 0.05) drug hits, which are sensitive in cells with an increased MYC expression. Drug hits were summarized in drug classes and compared with hits of our experimental drug screening in a Venn diagram.

PDAC transcriptome datasets of the cancer genome atlas (TCGA) were curated according to Peran *et al.* [34] (*n* = 150) and mRNA expression data and clinical data were accessed via the GDC data portal (https://portal.gdc.cancer.gov/) [35]. The international cancer gene consortium (ICGC) dataset was downloaded from the supplemental data of [7]. Acinar cell carcinomas and intraductal papillary mucinous neoplasms were excluded (*n* = 81). TCGA and ICGC datasets were clustered using ClustVis [36] using Euclidean for distance and the Ward method. The datasets were clustered according to the genes of the HALLMARK-MYC-TARGET_V1, HALLMARK-MYC-TARGET_V2, and the direct MYC targets determined by Muhar *et al.* [37]. PDAC identified by all three signatures were considered as common MYC^{high} PDACs. For the TCGA dataset clustered by HALLMARK-MYC-TARGET_V1, a cluster with incomplete high expression of the target genes was recognized and included in the MYC^{high} group according to this gene set. Survival data were assigned to the commonly MYC^{high} PDAC subtype and displayed in a Kaplan–Meier curve. For subtype association of the common MYC^{high} PDAC, the subtyping of Bailey *et al.* [7] was used and the pancreatic progenitor subtype, ADEX subtype, and the immunogenic subtype were combined and depicted as nonsquamous. The TCGA dataset was subtyped according to the identifier published by Moffitt *et al.* [38]. RNA-seq data of untreated and 4-OHT treated IMIM-PC1^{MYCER} cells were described [29] and can be accessed via NCBI/GEO: GSE119423. Enrichment analysis of gene sets was performed using the gene set enrichment analysis (GSEA) tool with default parameters (weighted) depending on sample size version 4.0.3 with signatures of the Molecular Signatures

Database v7.0 and the MYC target gene set from Muhar *et al.* [37]. The false discovery rate (FDR) *q*-values and normalized enrichment scores (ES) are depicted in the figures. The signature: ATF4 HUMAN TF ARCHS4 COEXPRESSION was downloaded via the EnrichR database [39]. In addition to the weighted GSEA, we performed an unweighted analysis of gene sets using the web tool GeneTrail2 1.6 [40]; multiple testing was corrected according to [41] and displayed as adjusted *P*-value.

2.2. Cell lines, CRISPR/Cas9-mediated knockout

Cell lines were cultured in high glucose Dulbecco's Modified Eagle Medium (DMEM; Sigma-Aldrich, Darmstadt, Germany) or RPMI (Life Technologies, Darmstadt, Germany) supplemented with 10% (v/v) FCS (Merck Millipore, Berlin, Germany) and 1% (v/v) penicillin/streptomycin (Life Technologies). All murine pancreatic cancer cell lines were established from $Kras^{G12D}$-driven mouse models of pancreatic cancer and cultivated as described [42]. Identity of the murine pancreatic cancer cell lines was verified by genotyping PCR. All human cell lines (Panc1, DanG, PaTu8988S, PSN1, PaTu8988T, MiaPaCa-2, IMIM-PC1, HPAC, HuPT4) were authenticated by Multiplexion (Multiplexion GmbH, Heidelberg, Germany). To screen for mycoplasma contamination, all cell lines are tested by PCR as described [43]. The dual recombinase system [44] was used to generate a murine PDAC cell line allowing to delete floxed *Myc* alleles [45] by a tamoxifen activatable Cre (CRE^{ERT2}). Alleles and genotyping for this murine PDAC cell line were recently described [46] and the PPT-MW1955 line corresponds to the following genotype: $Pdx1\text{-}Flp;FSF\text{-}Kras^{G12D/+}; FSF\text{-}R26^{CAG\text{-}CreERT2/+};Myc^{lox/lox}$. The murine cell line PPT-9091 was transduced with the pBabepuro-myc-ER construct, which was a gift from Wafik El-Deiry (Addgene plasmid # 19128; http://n2t.net/addgene: 19128; RRID:Addgene_19128) as described [29]. IMIM-PC1MYC^{ER} cells were described recently [29].

To generate the CRISPR/Cas9-mediated *NOXA* knockout, the protein coding region of *NOXA*s exon two was targeted by two sgRNAs (sg#1: T C G A G T G T G C T A C T C A A C T C; sg#2: T G T A A T T G A G A G G A A T G T G A), which were cloned into the pKLV-U6gRNA(BbsI)-PGKpuro-o2ABFP vector which was a gift from Kosuke Yusa (Addgene plasmid # 50946; http://n2t.net/addgene: 50946; RRID: Addgene_50946). MiaPaCa2 cells were co-transfected with a Cas9 expressing px330 vector and the two guides or the pKLV backbone only. Positive transfected MiaPaCa-2 cells were grown under

puromycin treatment (1 μg·mL^{-1}) for 2 weeks. Subsequently, single clones were generated, isolated, and screened via PCR for knockout clones. The primer set: C A C T A G T G T G G G C G T A T T A G G (FW) + G A T G T A T T C C A T C T T C C G T T T C C (RV1) reveals a product of 157 bp for knockout cells and 342 bp for wild-type cells (data not shown). To further test whether both alleles are deleted the primer set: FW + G T T C A G T T T G T C T C C A A A T C T C C (RV2) was used; here, a product at 137 bp is amplified if the cells harbor a *NOXA* allele and no product if the cells harbor a knockout for NOXA.

2.3. Cell lysis and western blot

To prepare whole-cell extracts RIPA buffer (50 mᴍ Tris, 150 mᴍ NaCl, 1% Nonidet P-40, 0.5% sodium deoxycholate, 0.1% SDS, pH 8.0) supplemented with protease and phosphatase inhibitors (protease inhibitor cocktail complete EDTA free; Roche Diagnostics, Mannheim, Germany, and Phosphatase-Inhibitor-Mix I; Serva, Heidelberg, Germany) was used. Whole-cell extracts were normalized for protein and heated at 95 °C for 5 min in protein loading buffer (45.6 mᴍ Tris/HCl pH 6.8, 2% SDS, 10% glycerol, 1% β-mercaptoethanol, 0.01% bromophenol blue) and loaded onto 10–12% SDS/PAGE and proteins were transferred to nitrocellulose membranes (Merck Millipore). Afterward, membranes were blocked in blocking buffer (5% skim milk, 0.1% Tween in PBS) and incubated with β-Actin (#A5316; Sigma-Aldrich), GAPDH (ACR001PS A160270BH; Acris, Herford, Germany), MYC (#9402; Cell Signaling, Danvers, MA, USA), NOXA (ALX-804-408-C100; Enzo Life Science, Farmingdale, NY, USA) and cleaved PARP (552596; BD Pharmingen, San Diego, CA, USA) primary antibodies. After overnight incubation (4 °C) with primary antibodies, membranes were incubated with DyLight™ 680 (#5366S; Cell Signaling) or 800 (#5151S; Cell Signaling) conjugated secondary antibodies (1 : 10 000 dilution). NOXA and GAPDH blots have been performed by chemiluminescence: secondary antibody Licor WesternSure® HRP goat anti-mouse IgG; substrate: Thermo Scientific SuperSignal™ West Pico PLUS Chemiluminescent Substrate (ThermoFisher, Darmstadt, Germany). Western blots were visualized by the Odyssey Infrared Imaging System (Licor, Bad Homburg, Germany) and quantified using the IMAGE STUDIO LITE Software V 5.2.5 (Licor). Cleaved PARP and MYC expression values were normalized on β-actin expression and final expression values were calculated out of three biological replicates.

2.4. Quantitative real-time PCR

To isolate RNA from cell lines, we followed the manufacturer's instructions of the Maxwell 16 LEV simply RNA Kit (# AS1280) (Promega, Walldorf, Germany). Quantification of mRNA was performed using the BRYT Green® Dye (GoTaq® qPCR, #A600A; Promega) in a real-time PCR analysis system (StepOne-Plus, Real-Time PCR System; Applied Biosystems Inc., Carlsbad, CA, USA). Primers used (5′–3′): *Myc*: T T C C T T T G G G C G T T G G A A A C (FW)/ G C T G T A C G G A G T C G T A G T C G (RV), *Odc1*: A C A T C C A A A G G C A A A G T T G G (FW)/ A G C C T G C T G G T T T T G A G T G T (RV), *Cad*: C T G C C C G G A T T G A T T G A T G T C (FW)/ G G T A T T A G G C A T A G C A C A A A C C A (RV) *Gapdh*: G G G T T C C T A T A A A T A C G G A C T G C (FW)/ T A C G G C C A A A T C C G T T C A C A (RV). Data analysis was carried out with StepOne software 2.3 Life Technologies/Applied Biosystems/ThermoFisher) by the $\Delta\Delta C_t$ method (as housekeeping gene *Gapdh* was used) as described [29].

2.5. Compounds

The anticancer compound library with $n = 129$ drugs was obtained as a plated compound set from the NCI/DTP Open Chemicals Repository (NCI/DTP, MD, USA); the full list of compounds is shown in Table S3. Bortezomib was purchased from LC-Laboratories (Woburn, MA, USA), marizomib was purchased from Cayman Chemicals (Ann Arbor, MI, USA), and 4-hydroxytamoxifen (4-OHT) was purchased from Sigma (Sigma, Munich, Germany).

2.6. Drug screening experiment

For the drug screen, we adapted a recent screening approach [47]. In an attempt to select for drugs highly active in PDAC, we screened PaTu-8988S, Panc1, DanG, and PSN1 cells with a single dose of 600 nM of each drug. Screening was conducted in a 96-well format. Twenty-four hours after the seeding (3000 cells per well), cells were treated with the drugs of the anticancer compound library for additional 72 h. Afterward, viability was measured with MTT assays as a read-out for the responsivity. The screen was performed as biological triplicates conducted as technical triplicates. The mean response in the MYC^high models was divided by the mean response in the MYC^low models. Drugs were ranked according to the ratio and a ratio > 2 was defined as a hit.

2.7. Viability assay, clonogenic assay, and caspase 3/7 assay

Thirty-eight recently characterized [48] murine PDAC cell lines driven by $Kras^{G12D/+}$ were termed as PDAC KC cell lines. Cell lines were seeded in a 96-well format. Twenty-four hours after the seeding (1500 cells per well), cells were treated with the respective drugs for additional 72 h. Afterward, viability was measured with MTT assays as a read-out for the responsivity. 3-(4,5-dimethylthiazol-2-yl)-2,5-diphenyltetrazolium bromide (Sigma, Munich) was used in a dilution of 5 mg·mL^{-1}. Ten microlitre of this MTT solution was added per well and incubated for 4 h at 37 °C. Subsequently, the medium was removed and the formazan crystals dissolved in 200 μL DMSO : EtOH (v/v) and incubated for 10 min on a horizontal shaker. Absorption was measured at 595 nm on a Thermo/LabSystem Multiskan RC Microplate Reader (Artisan Technology Group, Champaign, IL, USA).

In addition to MTT assay, cellular viability was measured by CellTiter-Glo ATP Viability Assay.

Briefly, 25 μL CellTiter-Glo® reagent purchased from Promega (Fitchburg, WI, USA) was added to each well of a 96-well plate 72 h after drug treatment. After 10 min of gentle shaking and 20 min of incubation at room temperature, luminescence was measured on a FLUOstar OPTIMA microplate reader (BMG Labtech, Ortenberg, Germany). The growth inhibitory 50% (GI_{50}) concentration was calculated with GRAPHPAD PRISM 6 (GraphPad Software, San Diego, CA, USA) using a nonlinear regression model. For the clonogenic assay, 2000 MiaPaCa-2 cells (wild-type or NOXA knockout) were seeded in 12-well plates. After 24 h, cells were treated once with the indicated doses of bortezomib followed by culturing for 14 days in DMEM (Sigma-Aldrich) supplemented with 10% (v/v) FCS (Merck Millipore) and 1% (v/v) penicillin/streptomycin (Life Technologies). Afterward, the medium was carefully removed, and cells were washed three times with PBS. The colonies were stained with 0.2% crystal violet solution (Sigma-Aldrich/Merck) for 20 min on a shaker at room temperature. To remove background staining, the wells were washed three times with tap water, dried, and subsequently visualized using a flatbed scanner. To determine activity of the effector caspases 3 and 7, we performed a luminescent-based Caspase-Glo 3/7 assay (G8090) from Promega (Fitchburg) and followed the manufacturers' instructions.

2.8. Statistical methods

All experiments were conducted in biological triplicates unless otherwise stated in the figure legends. ANOVA

or two-sided Student's *t*-test was used to investigate statistical significance, as indicated. *P*-values were calculated with GRAPHPAD PRISM 6/8 (GraphPad Software) and corrected according to Bonferroni for multiple testing unless otherwise indicated. *P*-values are indicated or * in the figures denotes $P < 0.05$. Fisher's exact test, was used to assess the association between PDAC subtypes and the expression of MYC target genes.

3. Results

3.1. Drug screening of FDA-approved anticancer drugs identifies vulnerabilities in MYC^high human PDAC cells

To identify vulnerabilities in PDACs with an increased MYC activity, we performed an unbiased pharmacological drug screening experiment. Based on publicly available transcriptional datasets (CCLE), we first identified cell lines with high and low MYC activity and selected four representative cell lines (two MYC^high, two MYC^low). Western blots of MYC^high cell lines demonstrated higher MYC protein expression and enrichment of relevant MYC signatures in GSEA of mRNA expression profiles (Fig. 1A). Except for PSN1, the doubling time of the cell lines was in similar ranges (Table S1). GSEA with the GeneTrail2 1.6 web service [40] demonstrated the activation of the MYC network in cells with higher expression of the protein (Fig. 1B). A novel gene set of direct MYC target genes defined by Muhar *et al.* [37] showed the strongest enrichment in the MYC^high cell lines (Fig. 1B). We used the described models for a drug screening experiment with a set of 129 FDA-approved anticancer drugs, which is outlined in Fig. 1C. Hits were determined as a twofold difference in the responsiveness of the MYC^high models. Among the ten candidates, we identified drugs from different classes, such as HDAC inhibitors, DNA antimetabolites, proteasome inhibitors, topoisomerase inhibitors, and others (Fig. 1D and Table S2).

3.2. Validation experiments confirm drug screening results

To validate the single-dose drug screening experiment, we again examined the top 11 hits of our screening experiment using different doses and determined the dose–response curves. In addition to the used screening platform, we included two more PDAC lines with low MYC protein expression (HPAC, HuPT4) and two PDAC lines with intermediate/high MYC expression (MiaPaCa2, PaTu8988T). As shown in Fig. 2A, MYC

protein expression is significantly different in the analyzed cell lines. Most dose–response curves were all left-shifted in the MYC^high models (Fig. 2B). Despite the low MYC expression in HPAC cells, these cells cluster into the MYC^high high group and show increased sensitivity, which could be explained by expression of functional wild-type p53. Although the mean area under the dose–response curves (AUC) is lower for all screening hits in the MYC^high models, a high variance was detected (Fig. 2B). Such observations point to the need for large cell line panels to ultimately validate screening hits. Therefore, to further substantiate the screening hits, we accessed the DoRothEA database [33]. This database links the transcriptional activity of 127 transcription factors to drug sensitivity. We accessed the data for MYC and found significant overlaps of six drug classes with our screening experiment, which points to the robustness of the screen (Fig. 2C).

3.3. MYC-associated pathways in human PDAC

To prioritize the hits of the screen, we accessed human PDAC mRNA expression datasets to observe potential connections of MYC-associated pathways to the screening hits. We used a PDAC data set from TCGA [35], which was curated according to Peran *et al.* ($n = 150$) [34]. In addition, we used the ICGC dataset [7], in which acinar cell carcinomas and intraductal papillary mucinous neoplasms were excluded ($n = 81$). We clustered both datasets according to the HALLMARK_MYC_TARGET_GENES_V1, the HALLMARK_MYC_TARGET_GENES_V2, and the MUHAR_MYC_TARGETS, as exemplified for the ICGC dataset in Fig. 3A. Eight cancers (~ 10%) were defined as MYC hyperactivated by all three MYC signatures (Fig. 3A,B). These cancers showed a reduced survival (Fig. S1A) and a clear connection to the squamous subtype of the disease (Figs 3A and S1B). Using the same approach for the TCGA dataset, 16 cancers (~ 10%) were defined to be MYC hyperactivated by all three used MYC signatures (Fig. S1C). Although survival of MYC hyperactivated cancers was not reduced in this dataset (Fig. S1D), a connection to the basal-like cancer was again observed (Fig. S1E), which confirms the documented connection of MYC to this subtype of PDAC [7,49]. To define MYC-associated pathways in the commonly MYC hyperactivated subtype, we performed a GSEA. Six hundred and three signatures were consistently enriched in both analyzed dataset when HALLMARKS-, KEGG-, GO-Term-, and REACTOME signatures were accessed via the MSigDB (Fig. 3C). Figure 3D shows HALLMARK and KEGG signatures linked to MYC in both
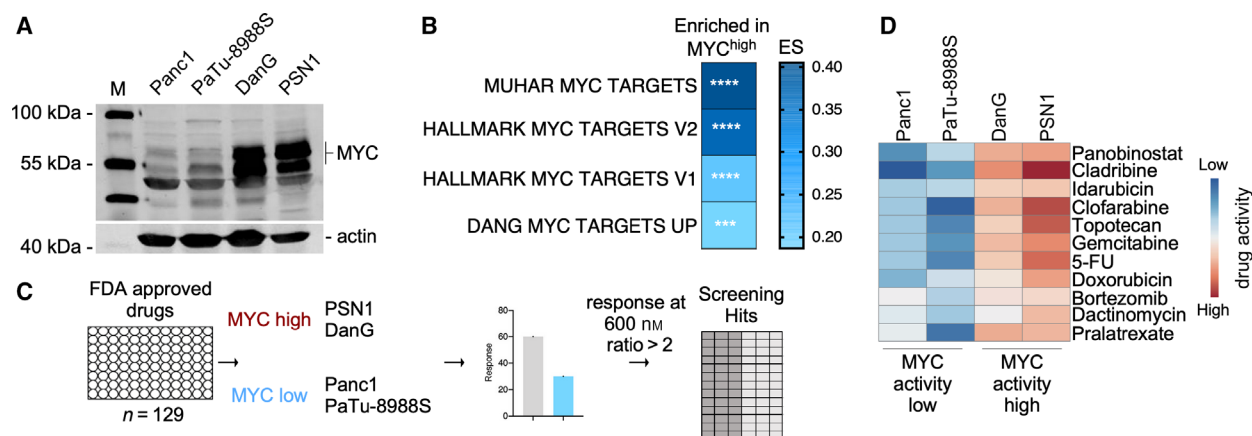
Fig. 1. Drug screening in human PDAC cells with diverse MYC activity. (A) MYC protein expression analysis of the four indicated PDAC cell lines was determined by western blotting. β-Actin (actin) served as a loading control. (B) GSEA by GeneTrail2 1.6 web service demonstrates enrichment of the depicted MYC signatures in the MYC[high] lines. Color-coded ES is depicted. *** adjusted *P* values < 0.001; **** adjusted *P* values < 0.0001. (C) Strategy for drug screening experiments with *n* = 129 FDA-approved anticancer drugs. Cells were treated for 72 h (two doubling times) with 600 nm of each compound. Hits were determined as a twofold difference in responsiveness. (D) Top 10 hits from the drug screening of 129 FDA-approved compounds depicted as a variance scaled heatmap.
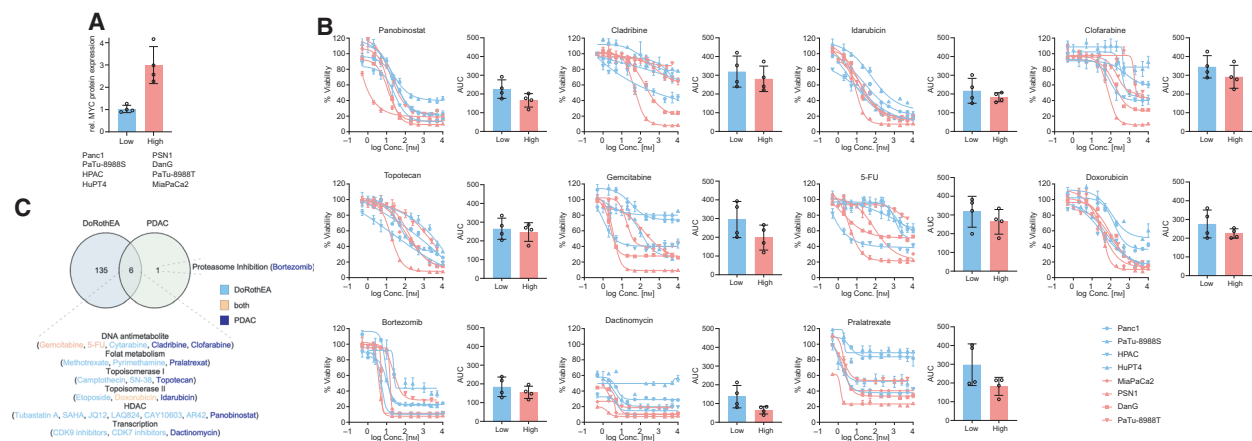

Fig. 2. Validation of the drug screening experiment. (A) Quantification of MYC expression of the indicated cell lines. In three independent lysates, the MYC expression was determined and shown is the mean with SD MYC expression per cell lines. *P* value of an unpaired *t*-test < 0.05. (B) Viability for multidose treatment of MYC[high] and MYC^{low} cells of displayed compounds. Cells were treated for 72 h and viability was measured by MTT. All experiments were conducted in *n* = 3 technical replicates in a dosage range of 0.5 nm–10 μm. Except for HPAC (*n* = 1), three independent biological replicates have been performed in the depicted cell lines. The mean (with SD) area under the dose–response curves (AUC) in both groups is depicted for each drug. (C) Venn diagram of data from the DoRothEA database and our drug screening hits. Significant (FDRq < 0.05) drug–MYC interactions of the DoRothEA database were compared to the hits of our experimental drug screening experiment. Drugs hits were summarized into drug classes.

datasets. To corroborate the direct connection of such pathways, we used a MYC estrogen receptor fusion protein (MYC[ER]) of IMIM-PC1 cells, which are characterized by low MYC protein abundance [29]. Here, MYC-activated signatures show an overlap to the HALLMARK and KEGG signatures detected in the analysis of the ICGC and TGCA datasets, pointing to direct effects of MYC (Fig. S1F). Investigating the

MYC-connected signatures, we detected a prominent proportion of ribosomal and translational signatures in both datasets, which is well in line with a recent analysis of the TCGA dataset demonstrating that translation is a key process linked to MYC in PDAC [50]. Consistent with increased translational activity, we detected signatures of the UPR and UPR-activated signaling, including protein kinase RNA-activated-like

ER kinase (PERK) and activating transcription factor 4 (ATF4) signatures in both investigated human PDAC datasets (Fig. 3E) [51].

3.4. MYC and sensitivity toward perturbants of protein homeostasis

The observation that MYC activity is connected to the UPR (Fig. 3D,E) and our recent demonstration that MYC is mechanistically involved in the induction of apoptosis in response to proteasome inhibition in PDAC cells [52], prompted us to investigate the bortezomib screening hit in greater detail. First, we used the dependency map (DepMap) portal to access bortezomib sensitivity data for PDAC cell lines using data from the PRISM repurposing primary screen [30], the GDSC2 screen [31], and the cancer target discovery and development network (CTD^2) screen [32]. We determined bortezomib-sensitive PDAC cell lines and analyzed them by a GSEA. Consistently, in all three datasets, we observed an enrichment of MYC signatures in the bortezomib-sensitive phenotype (Fig. 4A). To validate a connection of the MYC network to increased sensitivity toward proteasome inhibitors across species, we performed multidose drug screenings with the proteasome inhibitors marizomib and bortezomib in 38 well-characterized murine $Kras^{G12D}$-driven PDAC cell lines [48] (Fig. 4B). The GI$_{50}$ values of both inhibitors showed a significant correlation (Fig. 4B). We used RNA-seq data [48] of these murine PDAC lines and investigated enrichment of MYC signatures in bortezomib sensitive, marizomib sensitive, and lines sensitive to both proteasome inhibitors. We detected enrichment of the MUHAR MYC TARGETS and the HALLMARK-MYC TARGETS V2 signature enriched in all proteasome inhibitor-sensitive phenotypes (Fig. 4C). To test whether sensitivity of perturbants of the protein homeostasis is commonly connected to increased MYC activity, we analyzed the HSP90 inhibitors ganetespib and NMS-E973, and the valosin-containing protein (VCP)/p97 inhibitor NMS-873. Such inhibitors are able to induce ER stress and the UPR [53–56]. Two additional proteasome inhibitors, oprozomib and ixazomib, were included as controls. To investigate the connection of HSP90 inhibitors and p97 inhibitors to MYC, we used again the data of the PRISM repurposing primary screen [30]. In GSEA, HSP90 and p97 inhibitors sensitive PDAC cell lines enrich for MYC signatures and an UPR signature (Fig. S1B). The same was again observed for oprozomib- and ixazomib-sensitive lines (Fig. S1D). These data support the conclusion that MYC hyperactivated

PDACs are more sensitive to perturbants of the protein homeostasis.

3.5. Human PDAC cells with active MYC are primed for bortezomib-induced apoptosis

Previously, we described that bortezomib-induced apoptosis of PDAC cell lines is mediated by MYC-dependent activation of pro-death BCL2 family members, including NOXA (PMAIP1) [52]. To corroborate augmented apoptosis induction as the underlying principle for the increased sensitivity toward proteasome inhibition in MYC^{high} PDAC lines, we monitored cleavage of the caspase substrate PARP and NOXA expression over time. Only in MYC^{high} lines, a significant NOXA induction and associated cleavage of PARP was observed eight hours after the treatment (Fig. 4D). Twenty-four hours after the treatment, NOXA was expressed and caspases were also activated in MYC^{low} cell lines (Fig. 4D). Nevertheless, bortezomib-induced PARP cleavage and NOXA expression were always higher in MYC^{high} lines (Fig. 4E). Since the BH3-only pro-apoptotic BCL2 family member NOXA was recently described to contribute to bortezomib-induced apoptosis in PDAC cell lines [52], we induced a CRISPR-Cas9-mediated knockout of the *NOXA* gene in MiaPaCa2 cells (Fig. 4F). The therapeutic response toward bortezomib is distinctly reduced in *NOXA*-deficient MiaPaCa2 cells (Fig. 4G-J), demonstrating the relevance of the gene for the bortezomib-induced apoptosis.

To analyze the direct contribution of MYC to the proteasome inhibitor sensitivity, we used the dual recombination system [44] with floxed *Myc* alleles [45] to generate a genetic loss-of-function PDAC model (Fig. 5A). Activation of a Cre^{ERT2} fusion by the addition of 4-OHT in this murine PDAC cell lines deleted the floxed *Myc* alleles and reduces MYC protein expression to ~ 30% compared to controls (Fig. 5B, C). It is important to note that we were not able to generate a complete *MYC* knockout, due to the profound counter selection of recombination escapers, which underscores the importance of MYC as a target in PDAC. Nevertheless, the MYC-reduced population was less bortezomib sensitive (Fig. 5D). In addition, we used a conditional gain-of-function model relying on a MYC estrogen receptor fusion (MYC^{ER}). We transduced a murine PDAC cell line with low MYC expression. Upon treatment with 4-hydoxytamoxifen (4-OHT), the MYC targets *Odc1* and *Cad* were induced and endogenous *Myc* was repressed by its negative autoregulation (Fig. 5E). Seeding the cells in 4-OHT for 24 h followed by a 3-day treatment period
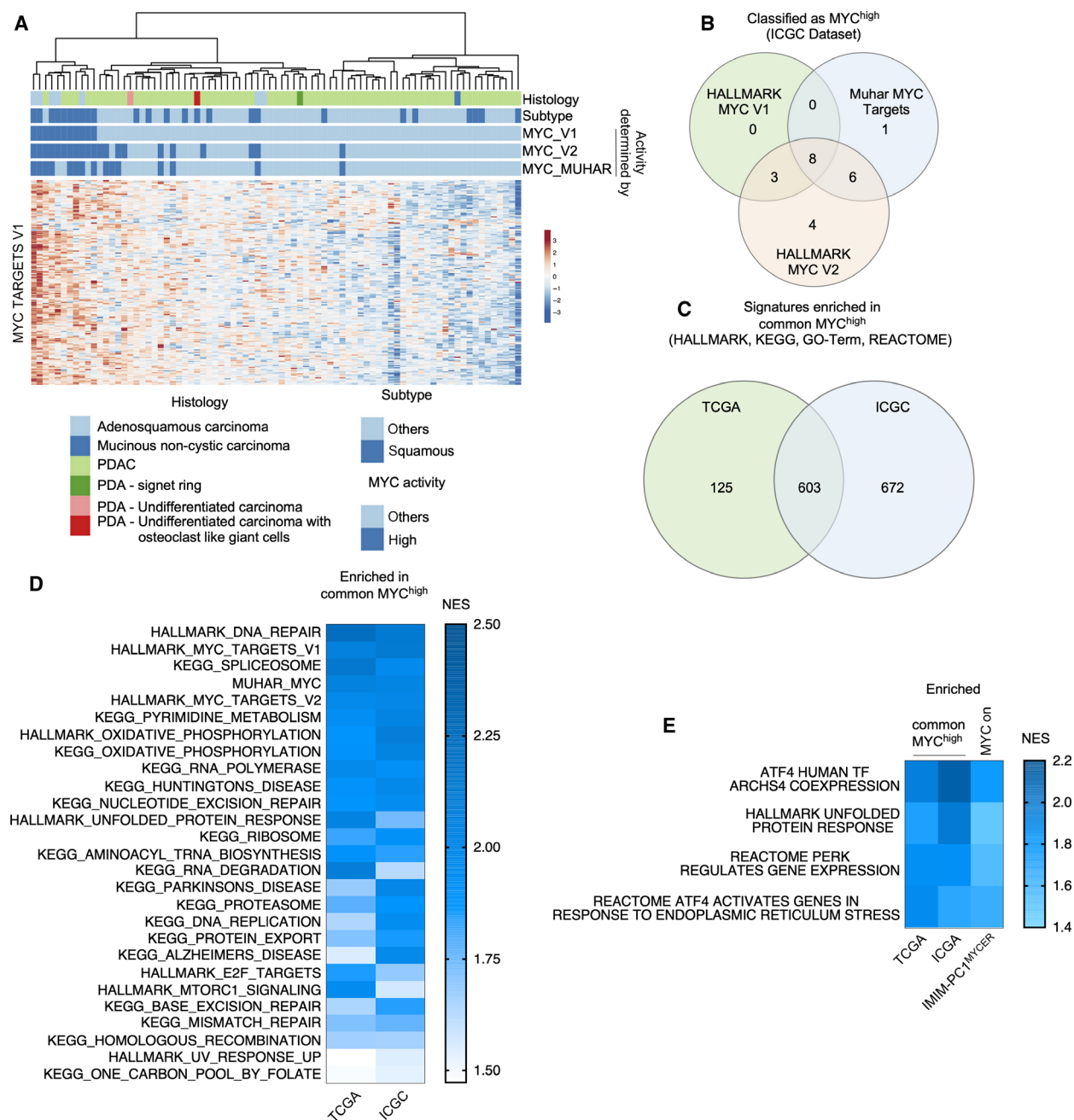
Fig. 3. Pathways enriched in human common MYC^high PDACs. (A) Clustering of the ICGC PDAC mRNA expression dataset according to the genes of the HALLMARK_MYC_TARGETS_V1 signature. Color-coded information of the histology, the subtype, and the MYC activity state determined by clustering of the HALLMARK_MYC_TARGETS_V1, the HALLMARK_MYC_TARGETS_V2, and the MUHAR MYC TARGETS [37] are depicted. (B) Venn diagram of PDAC identified as MYC^high by clustering of the genes of the depicted signatures in the ICGC dataset. Eight PDACs were identified as common MYC^high PDACs. (C) Common MYC^high PDACs of the TCGA and the ICGC dataset were analyzed by GSEA using the HALLMARK, the KEGG, the REACTOME, and the GO-TERM signatures of the MSigDB with a FDR *q* value threshold of < 0.25. The Venn diagram depicts 603 signatures enriched in common MYC^high PDACs of both datasets. (D) NES visualized by a heatmap of the HALLMARK and the KEGG signatures enriched in common MYC^high PDACs of both datasets. (E) NES visualized by a heatmap of gene signatures of the UPR and UPR-associated pathways enriched in common MYC^high PDACs of both datasets. As a control, IMIM-PC1^MYCER cells were used. Shown is the NES of the same signatures enriched in 4-OHT treated (MYC on) cells. For all depicted signatures: FDR *q* < 0.05.
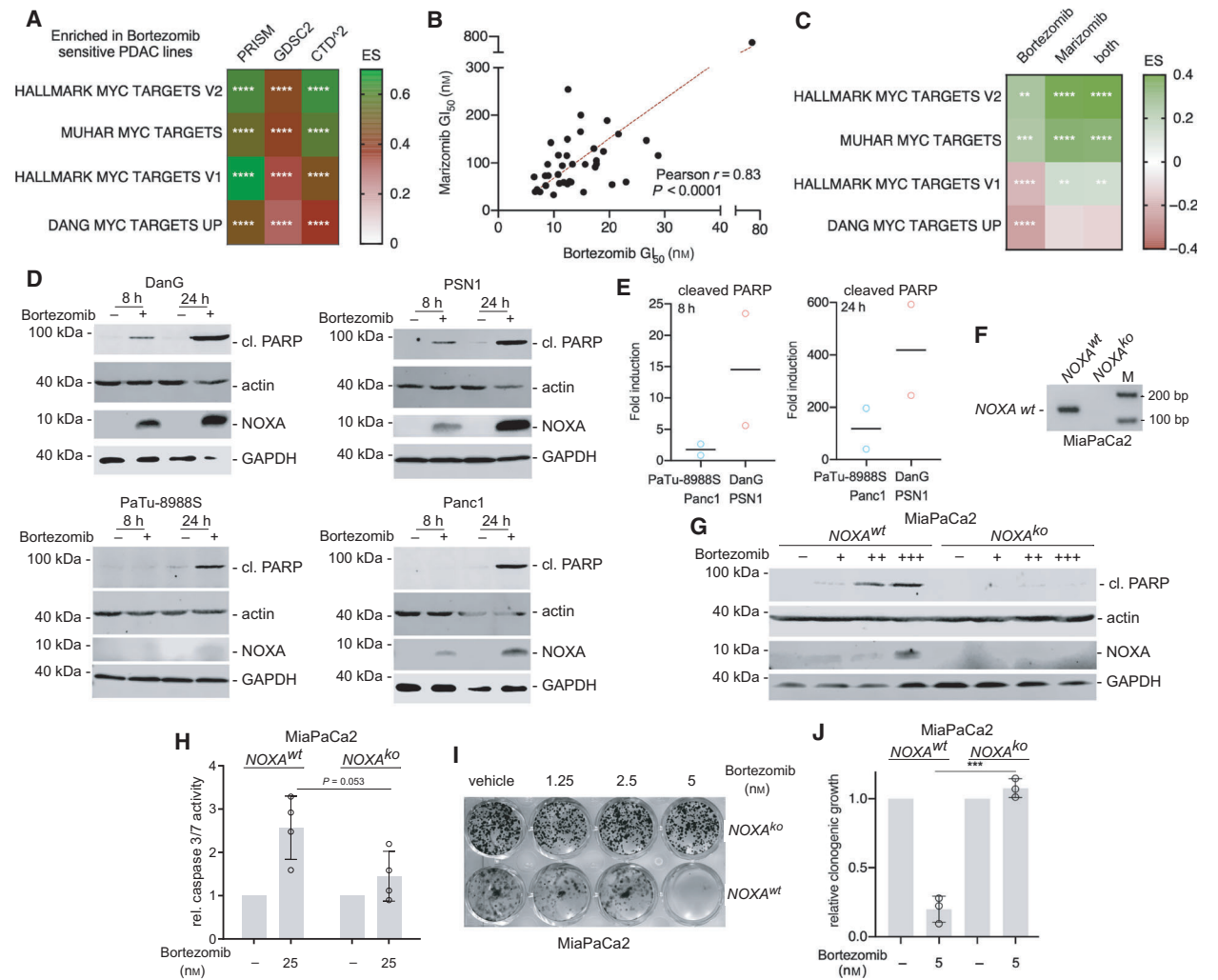
Fig. 4. MYC primes for proteasome inhibitor-induced apoptosis. (A) Bortezomib sensitivities of human PDAC cell lines from the PRISM repurposing primary screen (19Q3) [30], the GDSC2 screen (AUC) [31], and the CTD^2 (AUC) screen [32] were divided into quartiles and lines for the most sensitive quartile were compared to the remaining cell lines of the complete CCLE-PDAC dataset with a GSEA using the GeneTrail2 1.6 web service. The ES was color-coded. **** adjust. *P*-value < 0.0001. (B) Growth inhibitory 50% concentration of *n* = 38 murine PDAC cell lines for bortezomib and marizomib was determined (72 h of treatment, seven-point dilution, MTT assay, nonlinear regression, *n* = 3 independent biological replicates as technical triplicates). Depicted is the Pearson correlation coefficient and the linear regression (in red). (C) Bortezomib and marizomib GI_{50} values were divided into quartiles and lines from the most sensitive quartile were compared to the remaining cell lines by GSEA. In addition, the lines belonging to the bortezomib as well as the marizomib most sensitive quartile were compared to the rest of the lines by GSEA. GSEA was conducted by the GeneTrail2 1.6 web service. Color-coded ES is depicted. **adj. *P*-value < 0.01, ***adj. *P*-value < 0.001, ****adj. *P*-value < 0.0001. (D) Different lysates were blotted (western blot) to different membranes to determine expression of cleaved PARP, NOXA and β-actin (actin), or GAPDH as loading controls, 8 and 24 h after treatment with 50 nM bortezomib or DMSO (vehicle control). (*n* = 3). (E) The cleaved PARP band was quantified in three independent experiments and the mean fold induction of cleaved PARP expression in MYC^low and MYC^high subtypes is depicted. (F) Determination of CRISPR/Cas9 mediated knockout of the *NOXA* gene in MiaPaCa2 cells by PCR. A product size of 137 bp indicates the wild-type allele, while no product indicates NOXA knockout a cells as described in MM section. (G) Western blot analysis for expression of NOXA and cleaved PARP of MiaPaCa2 cells harboring either a *NOXA* wild-type expression or a *NOXA* knockout. β-Actin (actin) and GAPDH served as loading controls. Cells were treated for 24 h with bortezomib (+ 50 nM, ++ 100 nM, +++ 200 nM) or treated with DMSO as vehicle control (-). (H) Relative caspase 3/7 activity (mean with SD) of MiaPaCa2 *NOXA* wild-type versus *NOXA* knockout cells. Cells were treated for 24 h with bortezomib (25 nM) or treated with DMSO as vehicle control (-). (I) Clonogenic growth assay of bortezomib-treated MiaPaCa-2 NOXA knockouts and wild-type cells with the indicated concentrations. One representative experiment out of three is depicted. (J) Quantification of three independent clonogenic growth assays (mean with SD) according to I). *P* value of an unpaired *t*-test < 0.001.

with bortezomib did not change the sensitivity to the proteasome inhibitor (Fig. 5F). *MYC*-amplified PSN1 cells were included as a bortezomib-sensitive control. Considering the time needed to adapt the system to MYC, we followed two strategies. First, pretreating the cells with 4-OHT for 24 h followed by a 6-day treatment period with bortezomib, demonstrated increased sensitivity in the MYC 'on' state (Fig. 5G). Second, pretreating the cells with 4-OHT for 96 h followed by 72 h of bortezomib treatment also sensitized the cells to bortezomib (Fig. 5H). Therefore, gain- and loss-of-function models support the note that MYC modulates the proteasome inhibitor sensitivity of PDAC cells.

4. Discussion

Success of cancer therapeutics substantially differs due to a huge heterogeneity of human cancers, incomplete understanding how drugs mechanistically act, poorly described resistance mechanisms, or a lack of stratification for patients, which benefit from the therapy. As recently shown, deregulation of MYC is sufficient to promote PDAC progression in mice [57]. Furthermore, an aggressive PDAC subtype is associated with high MYC activity [7] and MYC-associated vulnerabilities can be exploited therapeutically [27,28,58]. Here, we performed a limited unbiased pharmacological screen and provide evidence that perturbants of the protein homeostasis are more effective in MYC-hyperactive PDAC cells.

Importantly, work from 2020 describes treatment options for PDAC using perturbants of the protein homeostasis in PDAC [59,60]. A subtype characterized by expression of cornified/squamous-related genes, the expression of ATF4 and CHOP, and sensitivity to the proteasome inhibitor carfilzomib was deciphered [59]. Although such data concur with our observations, an involvement of MYC was not investigated and the observation was more restricted to carfilzomib, than to other proteasome inhibitors [59].

Myelocytomatosis oncogene is well known to serve the metabolic demands for biomass accumulation of dividing cells, including a prominent function toward protein synthesis through increasing ribosome biogenesis [61]. The relevance of MYC-induced protein synthesis for its function in cancer is well documented. Ribosomal protein haploinsufficiency impairs MYCs oncogenic activity in the *Eμ-Myc* lymphoma model [62]. High MYC activity increases the protein load beyond the protein folding capacity of cells and can therefore activate UPR in mammalians and Drosophila [63,64]. The importance of MYC-induced UPR

is underscored by the demonstration of a synthetic lethal interaction of MYC with components of the UPR, including PERK and XBP1 [63,65,66]. Across several PDAC datasets and in mechanistic conditional MYC off/on models, we observed a connection of MYC activity to UPR signatures, arguing that PDACs with high MYC activity might be at the edge to die from proteotoxicity. Although such cancer cells can cope with the increased protein load via an adaptive ER stress-induced survival pathway [51], they are less able to tolerate any further increased protein challenge, contributing to our observation of increased proteasome inhibitor sensitivity in at least some MYC-hyperactive PDACs. Such a scenario is supported by several layers of evidence. It was demonstrated that PDAC cells escaping dependency on KRAS activate the MYC network to increase protein synthesis, which activates adaptive ER stress pathways [67]. Consistent with our data, such PDAC cells were found to be susceptible to perturbations of protein homeostasis induced by HSP90 or proteasome inhibitors [67]. Moreover, we found that human PDAC lines sensitive to the VCP/p97 inhibitor NMS-873, known to trigger a UPR [55,56], enrich for MYC signatures. The strong connection of MYC to translation, the observed link to the UPR, the enrichment of MYC signatures in p97 inhibitor or HSP90 inhibitor-sensitive PDAC cell lines, and the modulation of the proteasome inhibitor response in *MYC* genetic gain- and loss-of-function models [52], argues that MYC-hyperactive PDACs are more sensitive toward perturbations of the protein homeostasis. Although these considerations need additional validations in context of PDAC, they are supported from clinical data in multiple myeloma, where MYC seem to be connected to a benefit of proteasome inhibitor-based therapy [68,69].

Although there is ample evidence that MYC generates vulnerability toward perturbants of the protein homeostasis, it is important to note that MYC-independent pathways can also contribute. UPR can be induced via reactive oxygen species (ROS) whereas in this scenario the GRP78/PERK/NRF2 axis is required to keep cellular ROS levels low and thus prevent apoptosis signaling [70,71]. In PDAC Nrf2 is associated with cap-dependent mRNA translation and supports PDAC maintenance [72]. The association of such a ROS-NRF2 pathway to proteasome inhibitor sensitivity in context of PDAC remains to be demonstrated. In addition, well-described changes in NFκB signaling [73], downregulation of anti-apoptotic proteins such as XIAP or BCL2 [74,75] associated sensitivity to proteasome inhibitors, an inhibition of the NFκB signaling pathway [73], the associated downregulation of anti-
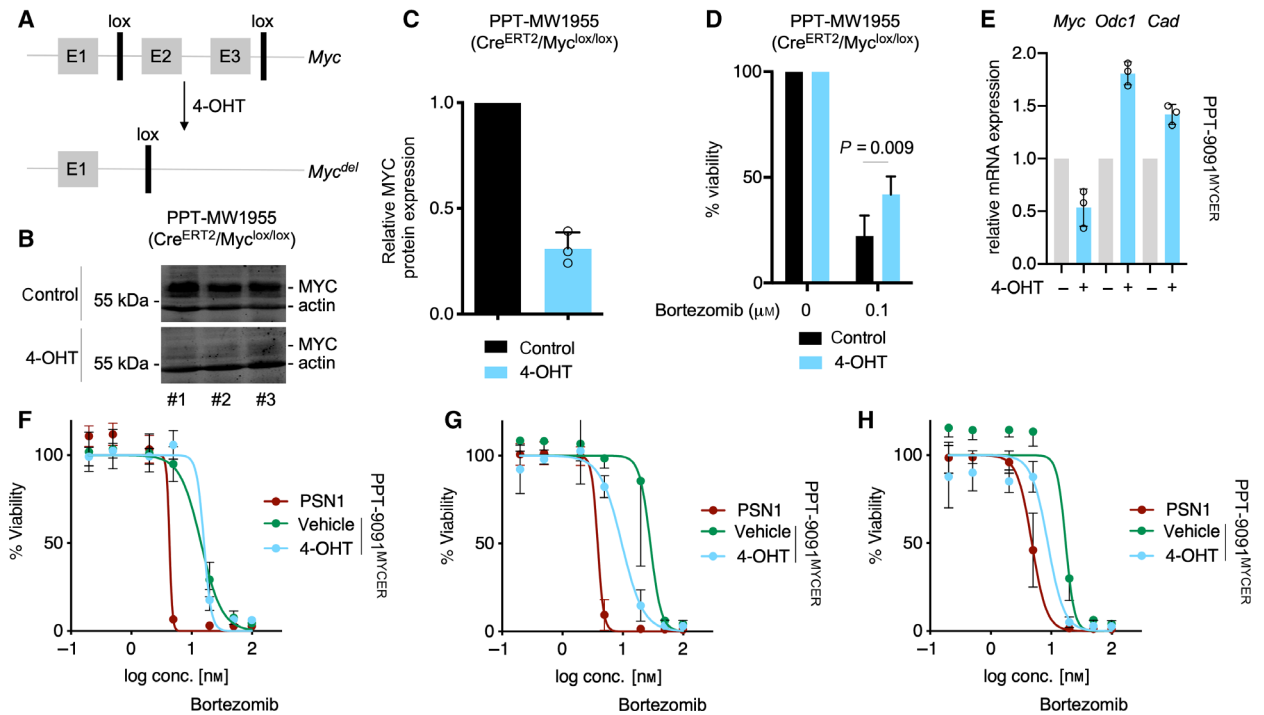
Fig. 5. Proteasome inhibitor sensitivity and MYC—genetic gain and loss of function. (A) Scheme of floxed *MYC* alleles, which can be deleted by Cre[ERT2] recombinase upon treatment with 4-OHT. E1-E3: Exon 1-Exon 3; 4-OHT: 4-OHT. (B) Protein expression of MYC and β-actin (actin, loading control) in EtOH and 4-OHT PDAC cells 72 h after treatment. Displayed are three independent biological replicates. (C) Quantification of MYC protein expression (mean with SD), determined by western blot ($n = 3$). (D) Relative viability of PDAC cells, 72 h after treatment with bortezomib. Cells were pretreated with EtOH and 4-OHT for 24 h. Viability was measured by MTT test. *P* value of an unpaired *t*-test is depicted (mean with SD; $n = 3$). (E) Quantitative PCR of indicated targets 72 h after treatment with 600 nM 4-OHT. *Gapdh* served as housekeeping control (mean with SD; $n = 3$). (F) Viability test by CellTiter-Glo of PSN1 and PPT-9091-MYC[ER] cell lines. Two thousand cells were seeded and after 24 h treated with 600 nM 4-OHT (MYC[ER] shuttles into nucleus) or EtOH (vehicle) and seven increasing concentrations of bortezomib for 3 days; highest conc.: 100 nM. (G) 6-day treatment with 600 nM of 4-OHT, and simultaneous treatment with bortezomib 24 h after seeding of 1000 cells/well similar to (F). (H) Treatment for 3 day with 600 nM 4-OHT and subsequent 3 day treatment with bortezomib without 4-OHT treatment according to (I). For F–H, the SD was used for error bars and three independent biological replicates were conducted as technical triplicates.

apoptotic proteins such as XIAP or BCL2 [74], the mutational status of the tumor suppressor p53 [76], and aneuploidy of the cancer cells [77] indicate increased responsivity toward proteasome inhibition.

Some PDAC xenograft *in vivo* models respond to proteasome inhibitor treatment [78,79], whereas others resist [80]. Also, for patient-derived xenografts (PdXs), proteasome inhibitor responding and nonresponding models have been documented [81,82]. Interestingly, Beglyarova *et al.* [82] observed a proteasome inhibitor response in a *MYC*-amplified PdX with high protein expression of the oncogene, whereas the nonamplified PdX tested in the study resisted the therapeutic intervention. Such observations clearly demonstrate the need to stratify for responsiveness toward perturbations of protein homeostasis and support our note that proteasome inhibitor sensitivity is a MYC/UPR-associated trait in PDAC. The lack of stratification might

contribute to the negative outcome of a phase II PDAC study, where patients were treated with bortezomib or with the combination containing gemcitabine and bortezomib [83].

In the neuroblastoma line SHEP, which harbors a *MYCN[ER]* transgene, an unbiased pharmacological screen with 938 FDA-approved drugs, recently demonstrated bortezomib, carfilzomib, cabazitaxel, pralatrexate, gemcitabine, vincristine, docetaxel, paclitaxel, etoposide, and doxorubicin to be the top ten MYCN-associated pharmacological vulnerabilities [84]. The substantial overlap of these hits with our screen validates the used experimental approach and demonstrates specific vulnerabilities across the MYC family and cross different tumor entities. As in the PDAC context, where MYC directly activates the transcription of the pro-death BCL2 family member *NOXA* (*PMAIP1*) [52] upon bortezomib treatment, NOXA

contributes also in neuroblastoma models significantly to the bortezomib-induced apoptosis [84].

The DoRothEA database [33] demonstrates that MYC has the highest number of transcription factor–drug interactions among all transcription factors analyzed [33]. Interestingly, only associations in which MYC is sensitizing for a drug were observed in this database [33]. Consistently, in context of PDAC, evidence that MYC increases the sensitivity toward proteasome inhibitors, BET inhibitors [27,28], SUMOylation inhibitors [29], the ERCC3 inhibitor triptolide [82], or cisplatin [85] was provided. However, it is important to note that MYC was also associated with drug resistance in PDAC. Important work has demonstrated that MYC is involved in a ductal-neuroendocrine lineage switch, whereby the neuroendocrine lineage resists gemcitabine [86]. Although paclitaxel was demonstrated to trigger a mitotic vulnerability [87], recent work, which investigated paclitaxel-resistant primary PDAC cultures implicates a MYC function in the resistant phenotype [88]. Interestingly, the anti-apoptotic BCL2 family member MCL1 is co-upregulated with MYC in paclitaxel-resistant PDAC cultures [88]. Anti-apoptotic BCL2 family members are described to be relevant modulators of the MYC-associated mitotic vulnerability [87]. Whether BCL2 family proteins are important switches, determining MYC-mediated sensitivity or resistance in the PDAC context awaits further detailed analysis.

5. Conclusions

As a mono- as well as in combination therapies, bortezomib demonstrates limited efficacy in solid cancers in the clinic [89–91]. Furthermore, a narrow therapeutic index and unfavorable pharmacokinetic features [89,91], with impaired distribution to solid tumors, may limit the clinical development of bortezomib in PDAC. However, our data provide evidence that perturbation of the protein homeostasis is an option to target MYC-active PDACs. Considering the development of next-generation proteasome inhibitors [89], the development of new bortezomib formulations [92], or options to target the ubiquitin–proteasome system at different levels [55,56,93], will allow to advance the concept in the future.

Acknowledgements

Conflict of interest

The authors declare no conflict of interest.

Data accessibility

Not applicable.

Author contributions

GS, MW, and CS designed the study, analyzed, and visualized the data and wrote the paper. KL, ZH, SL, MJD, CS, and RÖ performed, interpreted, and analyzed experiments and/or generated important model systems. DS., RR, UK, OHK, and MR provided important resources and critical input. All authors read and approved the final manuscript.

References

1 Siegel RL, Miller KD & Jemal A (2019) Cancer statistics, 2019. *CA Cancer J Clin* **69**, 7–34.

2 Collisson EA, Bailey P, Chang DK & Biankin AV (2019) Molecular subtypes of pancreatic cancer. *Nat Rev Gastroenterol Hepatol* **16**, 207–220.

3 Cancer Genome Atlas Research Network & Cancer Genome Atlas Research Network (2017) Integrated genomic characterization of pancreatic ductal adenocarcinoma. *Cancer Cell* **32**, 185–203.

4 Nicolle R, Blum Y, Marisa L, Loncle C, Gayet O, Moutardier V, Turrini O, Giovannini M, Bian B, Bigonnet M *et al.* (2017) Pancreatic adenocarcinoma therapeutic targets revealed by tumor-stroma cross-talk analyses in patient-derived xenografts. *Cell Rep* **21**, 2458–2470.

5 Noll EM, Eisen C, Stenzinger A, Espinet E, Muckenhuber A, Klein C, Vogel V, Klaus B, Nadler

W, Rosli C *et al.* (2016) CYP3A5 mediates basal and
acquired therapy resistance in different subtypes of
pancreatic ductal adenocarcinoma. *Nat Med* **22**, 278–
287.

6 Waddell N, Pajic M, Patch AM, Chang DK, Kassahn
KS, Bailey P, Johns AL, Miller D, Nones K, Quek K
et al. (2015) Whole genomes redefine the mutational
landscape of pancreatic cancer. *Nature* **518**, 495–501.

7 Bailey P, Chang DK, Nones K, Johns AL, Patch AM,
Gingras MC, Miller DK, Christ AN, Bruxner TJ,
Quinn MC *et al.* (2016) Genomic analyses identify
molecular subtypes of pancreatic cancer. *Nature* **531**,
47–52.

8 Daemen A, Peterson D, Sahu N, McCord R, Du X,
Liu B, Kowanetz K, Hong R, Moffat J, Gao M *et al.*
(2015) Metabolite profiling stratifies pancreatic ductal
adenocarcinomas into subtypes with distinct sensitivities
to metabolic inhibitors. *Proc Natl Acad Sci USA* **112**,
E4410–E4417.

9 Aung KL, Fischer SE, Denroche RE, Jang GH, Dodd
A, Creighton S, Southwood B, Liang SB, Chadwick D,
Zhang A *et al.* (2018) Genomics-driven precision
medicine for advanced pancreatic cancer: early results
from the COMPASS trial. *Clin Cancer Res* **24**, 1344–
1354.

10 Collisson EA, Sadanandam A, Olson P, Gibb WJ,
Truitt M, Gu S, Cooc J, Weinkle J, Kim GE, Jakkula
L *et al.* (2011) Subtypes of pancreatic ductal
adenocarcinoma and their differing responses to
therapy. *Nat Med* **17**, 500–503.

11 Muckenhuber A, Berger AK, Schlitter AM, Steiger K,
Konukiewitz B, Trumpp A, Eils R, Werner J, Friess H,
Esposito I *et al.* (2018) Pancreatic ductal
adenocarcinoma subtyping using the biomarkers
hepatocyte nuclear factor-1A and cytokeratin-81
correlates with outcome and treatment response. *Clin
Cancer Res* **24**, 351–359.

12 Tiriac H, Belleau P, Engle DD, Plenker D, Deschenes
A, Somerville TDD, Froeling FEM, Burkhart RA,
Denroche RE, Jang GH *et al.* (2018) Organoid profiling
identifies common responders to chemotherapy in
pancreatic cancer. *Cancer Discov* **8**, 1112–1129.

13 Karasinska JM, Topham JT, Kalloger SE, Jang GH,
Denroche RE, Culibrk L, Williamson LM, Wong HL,
Lee MKC, O'Kane GM *et al.* (2019) Altered gene
expression along the glycolysis-cholesterol synthesis axis
is associated with outcome in pancreatic cancer. *Clin
Cancer Res* **26**, 135–146.

14 Witkiewicz AK, McMillan EA, Balaji U, Baek G, Lin
WC, Mansour J, Mollaee M, Wagner KU, Koduru P,
Yopp A *et al.* (2015) Whole-exome sequencing of
pancreatic cancer defines genetic diversity and
therapeutic targets. *Nat Commun* **6**, 6744.

15 Dang CV (2012) MYC on the path to cancer. *Cell* **149**,
22–35.

16 Wirth M, Mahboobi S, Kramer OH & Schneider G
(2016) Concepts to target MYC in pancreatic cancer.
Mol Cancer Ther **15**, 1792–1798.

17 Wirth M & Schneider G (2016) MYC: a stratification
marker for pancreatic cancer therapy. *Trends Cancer* **2**,
1–3.

18 Hessmann E, Schneider G, Ellenrieder V & Siveke JT
(2016) MYC in pancreatic cancer: novel mechanistic
insights and their translation into therapeutic strategies.
Oncogene **35**, 1609–1618.

19 Allen-Petersen BL & Sears RC (2019) Mission possible:
advances in MYC therapeutic targeting in cancer.
BioDrugs **33**, 539–553.

20 Fletcher S & Prochownik EV (2015) Small-molecule
inhibitors of the Myc oncoprotein. *Biochim Biophys
Acta* **1849**, 525–543.

21 Huang A, Garraway LA, Ashworth A & Weber B
(2019) Synthetic lethality as an engine for cancer drug
target discovery. *Nat Rev Drug Discov* **19**, 23–38.

22 Cermelli S, Jang IS, Bernard B & Grandori C (2014)
Synthetic lethal screens as a means to understand and
treat MYC-driven cancers. *Cold Spring Harb Perspect
Med* **4**, a014209.

23 Herold S, Kalb J, Buchel G, Ade CP, Baluapuri A, Xu
J, Koster J, Solvie D, Carstensen A, Klotz C *et al.*
(2019) Recruitment of BRCA1 limits MYCN-driven
accumulation of stalled RNA polymerase. *Nature* **567**,
545–549.

24 Kessler JD, Kahle KT, Sun T, Meerbrey KL,
Schlabach MR, Schmitt EM, Skinner SO, Xu Q, Li
MZ, Hartman ZC *et al.* (2012) A SUMOylation-
dependent transcriptional subprogram is required for
Myc-driven tumorigenesis. *Science* **335**, 348–353.

25 Toyoshima M, Howie HL, Imakura M, Walsh RM,
Annis JE, Chang AN, Frazier J, Chau BN, Loboda A,
Linsley PS *et al.* (2012) Functional genomics identifies
therapeutic targets for MYC-driven cancer. *Proc Natl
Acad Sci USA* **109**, 9545–9550.

26 Hsieh AL & Dang CV (2016) MYC, metabolic
synthetic lethality, and cancer. *Recent Results Cancer
Res* **207**, 73–91.

27 Bian B, Bigonnet M, Gayet O, Loncle C, Maignan A,
Gilabert M, Moutardier V, Garcia S, Turrini O,
Delpero JR *et al.* (2017) Gene expression profiling of
patient-derived pancreatic cancer xenografts predicts
sensitivity to the BET bromodomain inhibitor JQ1:
implications for individualized medicine efforts. *EMBO
Mol Med* **9**, 482–497.

28 Bian B, Juiz NA, Gayet O, Bigonnet M, Brandone N,
Roques J, Cros J, Wang N, Dusetti N & Iovanna J
(2019) Pancreatic cancer organoids for determining
sensitivity to bromodomain and extra-terminal
inhibitors (BETi). *Front Oncol* **9**, 475.

29 Biederstädt A, Hassan Z, Schneeweis C, Schick M,
Schneider L, Muckenhuber A, Hong Y, Siegers G,

Nilsson L, Wirth M *et al.* (2020) SUMO pathway inhibition targets an aggressive pancreatic cancer subtype. *Gut* **69**, 1472–1482.

30 Corsello SM, Nagari RT, Spangler RD, Rossen J, Kocak M, Bryan JG, Humeidi R, Peck D, Wu X, Tang AA *et al.* (2019) Non-oncology drugs are a source of previously unappreciated anti-cancer activity. *bioRxiv.* "[PREPRINT]" https://doi.org/10.1101/730119.

31 Iorio F, Knijnenburg TA, Vis DJ, Bignell GR, Menden MP, Schubert M, Aben N, Goncalves E, Barthorpe S, Lightfoot H *et al.* (2016) A landscape of pharmacogenomic interactions in cancer. *Cell* **166**, 740–754.

32 Aksoy BA, Dancik V, Smith K, Mazerik JN, Ji Z, Gross B, Nikolova O, Jaber N, Califano A, Schreiber SL *et al.* (2017) CTD2 dashboard: a searchable web interface to connect validated results from the Cancer Target Discovery and Development Network. *Database* **2017**, bax054.

33 Garcia-Alonso L, Iorio F, Matchan A, Fonseca N, Jaaks P, Peat G, Pignatelli M, Falcone F, Benes CH, Dunham I *et al.* (2018) Transcription factor activities enhance markers of drug sensitivity in cancer. *Cancer Res* **78**, 769–780.

34 Peran I, Madhavan S, Byers SW & McCoy MD (2018) Curation of the pancreatic ductal adenocarcinoma subset of the cancer genome atlas is essential for accurate conclusions about survival-related molecular mechanisms. *Clin Cancer Res* **24**, 3813–3819.

35 Cancer Genome Atlas Research Netwok, Weinstein JN, Collisson EA, Mills GB, Shaw KR, Ozenberger BA, Ellrott K, Shmulevich I, Sander C & Stuart JM (2013) The cancer genome atlas pan-cancer analysis project. *Nat Genet* **45**, 1113–1120.

36 Metsalu T & Vilo J (2015) ClustVis: a web tool for visualizing clustering of multivariate data using Principal Component Analysis and heatmap. *Nucleic Acids Res* **43**, W566–W570.

37 Muhar M, Ebert A, Neumann T, Umkehrer C, Jude J, Wieshofer C, Rescheneder P, Lipp JJ, Herzog VA, Reichholf B *et al.* (2018) SLAM-seq defines direct gene-regulatory functions of the BRD4-MYC axis. *Science* **360**, 800–805.

38 Moffitt RA, Marayati R, Flate EL, Volmar KE, Loeza SG, Hoadley KA, Rashid NU, Williams LA, Eaton SC, Chung AH *et al.* (2015) Virtual microdissection identifies distinct tumor- and stroma-specific subtypes of pancreatic ductal adenocarcinoma. *Nat Genet* **47**, 1168–1178.

39 Kuleshov MV, Jones MR, Rouillard AD, Fernandez NF, Duan Q, Wang Z, Koplev S, Jenkins SL, Jagodnik KM, Lachmann A *et al.* (2016) Enrichr: a comprehensive gene set enrichment analysis web server 2016 update. *Nucleic Acids Res* **44**, W90–W97.

40 Stockel D, Kehl T, Trampert P, Schneider L, Backes C, Ludwig N, Gerasch A, Kaufmann M, Gessler M, Graf N *et al.* (2016) Multi-omics enrichment analysis using the GeneTrail2 web service. *Bioinformatics* **32**, 1502–1508.

41 Benjamini Y, Drai D, Elmer G, Kafkafi N & Golani I (2001) Controlling the false discovery rate in behavior genetics research. *Behav Brain Res* **125**, 279–284.

42 von Burstin J, Eser S, Paul MC, Seidler B, Brandl M, Messer M, von Werder A, Schmidt A, Mages J, Pagel P *et al.* (2009) E-cadherin regulates metastasis of pancreatic cancer *in vivo* and is suppressed by a SNAIL/HDAC1/HDAC2 repressor complex. *Gastroenterology* **137**, 361–371.

43 Ossewaarde JM, de Vries A, Bestebroer T & Angulo AF (1996) Application of a Mycoplasma group-specific PCR for monitoring decontamination of Mycoplasma-infected *Chlamydia* sp. strains. *Appl Environ Microbiol* **62**, 328–331.

44 Schonhuber N, Seidler B, Schuck K, Veltkamp C, Schachtler C, Zukowska M, Eser S, Feyerabend TB, Paul MC, Eser P *et al.* (2014) A next-generation dual-recombinase system for time- and host-specific targeting of pancreatic cancer. *Nat Med* **20**, 1340–1347.

45 de Alboran IM, O'Hagan RC, Gartner F, Malynn B, Davidson L, Rickert R, Rajewsky K, DePinho RA & Alt FW (2001) Analysis of C-MYC function in normal cells via conditional gene-targeted mutation. *Immunity* **14**, 45–55.

46 Diersch S, Wirth M, Schneeweis C, Jors S, Geisler F, Siveke JT, Rad R, Schmid RM, Saur D, Rustgi AK *et al.* (2016) Kras(G12D) induces EGFR-MYC cross signaling in murine primary pancreatic ductal epithelial cells. *Oncogene* **35**, 3880–3886.

47 Christensen CL, Kwiatkowski N, Abraham BJ, Carretero J, Al-Shahrour F, Zhang T, Chipumuro E, Herter-Sprie GS, Akbay EA, Altabef A *et al.* (2014) Targeting transcriptional addictions in small cell lung cancer with a covalent CDK7 inhibitor. *Cancer Cell* **26**, 909–922.

48 Mueller S, Engleitner T, Maresch R, Zukowska M, Lange S, Kaltenbacher T, Konukiewitz B, Ollinger R, Zwiebel M, Strong A *et al.* (2018) Evolutionary routes and KRAS dosage define pancreatic cancer phenotypes. *Nature* **554**, 62–68.

49 Chan-Seng-Yue M, Kim JC, Wilson GW, Ng K, Figueroa EF, O'Kane GM, Connor AA, Denroche RE, Grant RC, McLeod J *et al.* (2020) Transcription phenotypes of pancreatic cancer are driven by genomic events during tumor evolution. *Nat Genet* **52**, 231–240.

50 Schaub FX, Dhankani V, Berger AC, Trivedi M, Richardson AB, Shaw R, Zhao W, Zhang X, Ventura A, Liu Y *et al.* (2018) Pan-cancer alterations of the MYC oncogene and its proximal network across the cancer genome atlas. *Cell Syst* **6**, 282–300.

51 Madden E, Logue SE, Healy SJ, Manie S& Samali A (2019) The role of the unfolded protein response in cancer progression: from oncogenesis to chemoresistance. *Biol Cell* **111**, 1–17.

52 Wirth M, Stojanovic N, Christian J, Paul MC, Stauber RH, Schmid RM, Hacker G, Kramer OH, Saur D& Schneider G (2014) MYC and EGR1 synergize to trigger tumor cell death by controlling NOXA and BIM transcription upon treatment with the proteasome inhibitor bortezomib. *Nucleic Acids Res* **42**, 10433–10447.

53 Davenport EL, Moore HE, Dunlop AS, Sharp SY, Workman P, Morgan GJ & Davies FE (2007) Heat shock protein inhibition is associated with activation of the unfolded protein response pathway in myeloma plasma cells. *Blood* **110**, 2641–2649.

54 Gallerne C, Prola A & Lemaire C (2013) Hsp90 inhibition by PU-H71 induces apoptosis through endoplasmic reticulum stress and mitochondrial pathway in cancer cells and overcomes the resistance conferred by Bcl-2. *Biochim Biophys Acta* **1833**, 1356–1366.

55 Vekaria PH, Home T, Weir S, Schoenen FJ & Rao R (2016) Targeting p97 to disrupt protein homeostasis in cancer. *Front Oncol* **6**, 181.

56 Magnaghi P, D'Alessio R, Valsasina B, Avanzi N, Rizzi S, Asa D, Gasparri F, Cozzi L, Cucchi U, Orrenius C *et al.* (2013) Covalent and allosteric inhibitors of the ATPase VCP/p97 induce cancer cell death. *Nat Chem Biol* **9**, 548–556.

57 Sodir NM, Kortlever RM, Barthet VJA, Campos T, Pellegrinet L, Kupczak S, Anastasiou P, Swigart LB, Soucek L, Arends MJ *et al.* (2020) MYC instructs and maintains pancreatic adenocarcinoma phenotype. *Cancer Discov* **10**, 588–607.

58 Biederstadt A, Hassan Z, Schneeweis C, Schick M, Schneider L, Muckenhuber A, Hong Y, Siegers G, Nilsson L, Wirth M *et al.* (2020) SUMO pathway inhibition targets an aggressive pancreatic cancer subtype. *Gut* **69**, 1472–1482.

59 Fraunhoffer NA, Abuelafia AM, Bigonnet M, Gayet O, Roques J, Telle E, Santofimia-Castano P, Borrello MT, Chuluyan E, Dusetti N *et al.* (2020) Evidencing a pancreatic ductal adenocarcinoma subpopulation sensitive to the proteasome inhibitor carfilzomib. *Clin Cancer Res* **26**, 5506–5519.

60 Liu Y, Awadia S, Delaney A, Sitto M, Engelke CG, Patel H, Calcaterra A, Zelenka-Wang S, Lee H, Contessa J *et al.* (2020) UAE1 inhibition mediates the unfolded protein response, DNA damage and caspase-dependent cell death in pancreatic cancer. *Transl Oncol* **13**, 100834.

61 Wolpaw AJ & Dang CV (2018) MYC-induced metabolic stress and tumorigenesis. *Biochim Biophys Acta Rev Cancer* **1870**, 43–50.

62 Barna M, Pusic A, Zollo O, Costa M, Kondrashov N, Rego E, Rao PH & Ruggero D (2008) Suppression of Myc oncogenic activity by ribosomal protein haploinsufficiency. *Nature* **456**, 971–975.

63 Hart LS, Cunningham JT, Datta T, Dey S, Tameire F, Lehman SL, Qiu B, Zhang H, Cerniglia G, Bi M *et al.* (2012) ER stress-mediated autophagy promotes Myc-dependent transformation and tumor growth. *J Clin Invest* **122**, 4621–4634.

64 Nagy P, Varga A, Pircs K, Hegedűs K & Juhász G (2013) Myc-driven overgrowth requires unfolded protein response-mediated induction of autophagy and antioxidant responses in *Drosophila melanogaster*. *PLoS Genet* **9**, e1003664.

65 Zhao N, Cao J, Xu L, Tang Q, Dobrolecki LE, Lv X, Talukdar M, Lu Y, Wang X, Hu DZ *et al.* (2018) Pharmacological targeting of MYC-regulated IRE1/XBP1 pathway suppresses MYC-driven breast cancer. *J Clin Invest* **128**, 1283–1299.

66 Xie H, Tang CH, Song JH, Mancuso A, Del Valle JR, Cao J, Xiang Y, Dang CV, Lan R, Sanchez DJ *et al.* (2018) IRE1alpha RNase-dependent lipid homeostasis promotes survival in Myc-transformed cancers. *J Clin Invest* **128**, 1300–1316.

67 Genovese G, Carugo A, Tepper J, Robinson FS, Li L, Svelto M, Nezi L, Corti D, Minelli R, Pettazzoni P *et al.* (2017) Synthetic vulnerabilities of mesenchymal subpopulations in pancreatic cancer. *Nature* **542**, 362–366.

68 Chng WJ, Huang GF, Chung TH, Ng SB, Gonzalez-Paz N, Troska-Price T, Mulligan G, Chesi M, Bergsagel Pl & Fonseca R (2011) Clinical and biological implications of MYC activation: a common difference between MGUS and newly diagnosed multiple myeloma. *Leukemia* **25**, 1026–1035.

69 Di Bacco A, Bahlis NJ, Munshi NC, Avet-Loiseau H, Masszi T, Viterbo L, Pour L, Ganly P, Cavo M, Langer C *et al.* (2020) c-MYC expression and maturity phenotypes are associated with outcome benefit from addition of ixazomib to lenalidomide-dexamethasone in myeloma. *Eur J Haematol* **105**, 35–46.

70 Chang CW, Chen YS, Tsay YG, Han CL, Chen YJ, Yang CC, Hung KF, Lin CH, Huang TY, Kao SY *et al.* (2018) ROS-independent ER stress-mediated NRF2 activation promotes warburg effect to maintain stemness-associated properties of cancer-initiating cells. *Cell Death Dis* **9**, 194.

71 Zinszner H, Kuroda M, Wang X, Batchvarova N, Lightfoot RT, Remotti H, Stevens JL & Ron D (1998) CHOP is implicated in programmed cell death in response to impaired function of the endoplasmic reticulum. *Genes Dev* **12**, 982–995.

72 Chio IIC, Jafarnejad SM, Ponz-Sarvise M, Park Y, Rivera K, Palm W, Wilson J, Sangar V, Hao Y, Ohlund D *et al.* (2016) NRF2 promotes tumor maintenance by modulating mRNA translation in pancreatic cancer. *Cell* **166**, 963–976.

73 Hideshima T, Ikeda H, Chauhan D, Okawa Y, Raje N, Podar K, Mitsiades C, Munshi NC, Richardson PG, Carrasco RD *et al.* (2009) Bortezomib induces canonical nuclear factor-kappaB activation in multiple myeloma cells. *Blood* **114**, 1046–1052.

74 Mitsiades N, Mitsiades CS, Poulaki V, Chauhan D, Fanourakis G, Gu X, Bailey C, Joseph M, Libermann TA, Treon SP *et al.* (2002) Molecular sequelae of proteasome inhibition in human multiple myeloma cells. *Proc Natl Acad Sci USA* **99**, 14374–14379.

75 Fennell DA, Chacko A & Mutti L (2008) BCL-2 family regulation by the 20S proteasome inhibitor bortezomib. *Oncogene* **27**, 1189–1197.

76 Chen S, Blank JL, Peters T, Liu XJ, Rappoli DM, Pickard MD, Menon S, Yu J, Driscoll DL, Lingaraj T *et al.* (2010) Genome-wide siRNA screen for modulators of cell death induced by proteasome inhibitor bortezomib. *Cancer Res* **70**, 4318–4326.

77 Chunduri NK & Storchová Z (2019) The diverse consequences of aneuploidy. *Nat Cell Biol* **21**, 54–62.

78 Nawrocki ST, Sweeney-Gotsch B, Takamori R & McConkey DJ (2004) The proteasome inhibitor bortezomib enhances the activity of docetaxel in orthotopic human pancreatic tumor xenografts. *Mol Cancer Ther* **3**, 59–70.

79 Sloss CM, Wang F, Liu R, Xia L, Houston M, Ljungman D, Palladino MA & Cusack JC Jr (2008) Proteasome inhibition activates epidermal growth factor receptor (EGFR) and EGFR-independent mitogenic kinase signaling pathways in pancreatic cancer cells. *Clin Cancer Res* **14**, 5116–5123.

80 Marten A, Zeiss N, Serba S, Mehrle S, von Lilienfeld-Toal M & Schmidt J (2008) Bortezomib is ineffective in an orthotopic mouse model of pancreatic adenocarcinoma. *Mol Cancer Ther* **7**, 3624–3631.

81 Kawaguchi K, Igarashi K, Murakami T, Kiyuna T, Lwin TM, Hwang HK, Delong JC, Clary BM, Bouvet M, Unno M *et al.* (2017) MEK inhibitors cobimetinib and trametinib, regressed a gemcitabine-resistant pancreatic-cancer patient-derived orthotopic xenograft (PDOX). *Oncotarget* **8**, 47490–47496.

82 Beglyarova N, Banina E, Zhou Y, Mukhamadeeva R, Andrianov G, Bobrov E, Lysenko E, Skobeleva N, Gabitova L, Restifo D *et al.* (2016) Screening of conditionally reprogrammed patient-derived carcinoma cells identifies ERCC3-MYC interactions as a target in pancreatic cancer. *Clin Cancer Res* **22**, 6153–6163.

83 Alberts SR, Foster NR, Morton RF, Kugler J, Schaefer P, Wiesenfeld M, Fitch TR, Steen P, Kim GP & Gill S (2005) PS-341 and gemcitabine in patients with metastatic pancreatic adenocarcinoma: a North Central Cancer Treatment Group (NCCTG) randomized phase II study. *Ann Oncol* **16**, 1654–1661.

84 Wang J, Jiang J, Chen H, Wang L, Guo H, Yang L, Xiao D, Qing G & Liu H (2019) FDA-approved drug screen identifies proteasome as a synthetic lethal target in MYC-driven neuroblastoma. *Oncogene* **38**, 6737–6751.

85 Biliran H Jr, Banerjee S, Thakur A, Sarkar FH, Bollig A, Ahmed F, Wu J, Sun Y & Liao JD (2007) c-Myc-induced chemosensitization is mediated by suppression of cyclin D1 expression and nuclear factor-kappa B activity in pancreatic cancer cells. *Clin Cancer Res* **13**, 2811–2821.

86 Farrell AS, Joly MM, Allen-Petersen BL, Worth PJ, Lanciault C, Sauer D, Link J, Pelz C, Heiser LM, Morton JP *et al.* (2017) MYC regulates ductal-neuroendocrine lineage plasticity in pancreatic ductal adenocarcinoma associated with poor outcome and chemoresistance. *Nat Commun* **8**, 1728.

87 Topham C, Tighe A, Ly P, Bennett A, Sloss O, Nelson L, Ridgway RA, Huels D, Littler S, Schandl C *et al.* (2015) MYC is a major determinant of mitotic cell fate. *Cancer Cell* **28**, 129–140.

88 Parasido E, Avetian GS, Naeem A, Graham G, Pishvaian M, Glasgow E, Mudambi S, Lee Y, Ihemelandu C, Choudhry M *et al.* (2019) The sustained induction of c-MYC drives Nab-paclitaxel resistance in primary pancreatic ductal carcinoma cells. *Mol Cancer Res* **17**, 1815–1827.

89 Manasanch EE & Orlowski RZ (2017) Proteasome inhibitors in cancer therapy. *Nat Rev Clin Oncol* **14**, 417–433.

90 Huang Z, Wu Y, Zhou X, Xu J, Zhu W, Shu Y & Liu P (2014) Efficacy of therapy with bortezomib in solid tumors: a review based on 32 clinical trials. *Future Oncol* **10**, 1795–1807.

91 Thibaudeau TA & Smith DM (2019) A practical review of proteasome pharmacology. *Pharmacol Rev* **71**, 170–197.

92 Deshantri AK, Metselaar JM, Zagkou S, Storm G, Mandhane SN, Fens MHAM & Schiffelers RM (2019) Development and characterization of liposomal formulation of bortezomib. *Int J Pharm X* **1**, 100011.

93 Best S, Hashiguchi T, Kittai A, Bruss N, Paiva C, Okada C, Liu T, Berger A & Danilov AV (2019) Targeting ubiquitin-activating enzyme induces ER stress-mediated apoptosis in B-cell lymphoma cells. *Blood Adv* **3**, 51–62.

Supporting information

Additional supporting information may be found online in the Supporting Information section at the end of the article.

Fig. S1. Survival and Subtypes of common MYC^{high} PDACs. A) Survival data of common MYC^{high} PDACs of the ICGC dataset are displayed in a Kaplan–Meier curve. *P* value of a log-rank test is depicted. B) Percentage of squamous subtype of the common MYC^{high} PDACs compared to the others. Fisher Exact test: *P* < 0.0001. C) Venn diagram of

PDAC identified as MYC[high] by clustering of the genes of the depicted signatures in the TCGA dataset. 16 PDACs were identified as common MYC[high] PDACs. D) Survival data of common MYC[high] PDACs of the TCGA dataset are displayed in a Kaplan–Meier curve. E) Percentage of basal-like subtype of the common MYC[high] PDACs compared to the others. Fisher Exact test: $P < 0.05$. F) GSEA of IMIM-PC1[MYCER] cells treated with 4-OHT to activate MYC. Depicted are HALLMARK and KEGG signature corresponding to the tissue-based analysis corresponding to Fig. 3D. The NES and the FDR q values are depicted.

Fig. S2. Association of MYC with perturbants of the protein homeostasis. Sensitivities of human PDAC cell lines from the PRISM repurposing primary screen (19Q3) [30] of the depicted drug classes were divided into quartiles and lines for the most sensitive quartile were compared to the remaining cell lines of the complete CCLE-PDAC dataset with a gene set enrichment analysis using the GeneTrail2 1.6 web service. The enrichment score was color-coded. ** adjust. P-value < 0.01; **** adjust. P-value < 0.0001.

Table S1. Doubling time of PDAC cell lines used for the drug screening experiment. Panc1, PaTu8988S, DanG and PSN1 cells were seeded in 96 well plates at a density of 3000 cells/well. After 24, 48, 72 and 96 h viable cells were measured by MTT test to determine doubling time of the cell lines.

Table S2. Complete list of the response to compounds used in the drug screen. PSN1, Panc1, PaTu8988S and DanG cells were treated with $n = 129$ compounds in biological and technical triplicates. Drug response as well as mean of MYC high and mean of MYC low are displayed.

Table S3. Pathways associated with MYC in common MYC[high] PDAC. GSEA of pathways enriched in common MYC[high] PDAC of the ICGC and the TCGA dataset.